Arabian Journal of Geosciences (2023) 16:335
https://doi.org/10.1007/s12517-023-11426-w

ORIGINAL PAPER

Geochemical insight on gem opal formation and highly weathered rhyolitic ignimbrite layer from Delanta area, south Wollo, northern Ethiopia

Mulugeta Milkias[1,2] · Tesfaye Demissie[1,2] · Daniel Meshesha[1,2]

Received: 16 December 2021 / Accepted: 15 April 2023 / Published online: 24 April 2023

Abstract
A large amount of gem-quality opals is found in south Wollo/Delanta woreda, especially in Wegel Tena and Tsehay Mewucha localities in central Ethiopia. Petrographic investigation shows the host rock comprises porphyritic rhyolitic ignimbrite with quartz, plagioclase, and alkali feldspar phenocrysts. The matrix is composed of glass shards and is mostly weathered into clay, with a small proportion of biotite, hornblende, opaque minerals, and lithic fragments. Geochemically, the rhyolitic ignimbrite displays a pattern typical of silicic volcanic rocks from the area, with depletions of Ba, K, Sr, P, and Ti due to feldspar, apatite, and Fe-Ti oxide crystal fractionation. The rhyolitic ignimbrite is characterized by light REE-enrichment pattern ($(La/Lu)_N = 7.05–14.65$) with slight negative Eu anomalies. The opal samples show lower REE than the rhyolitic ignimbrite, with stronger negative Eu anomalies and more positive Ce anomalies than the host rhyolitic ignimbrite. The Eu and Ce anomalies indicate that the fluid responsible for opal precipitation is associated in part with feldspar dissolution under variations in redox conditions, respectively. Therefore, as demonstrated in previous studies, we concluded that the Delanta opal is formed through intense weathering and alteration of rhyolitic ignimbrite before the eruption of the overlying thick and welded rhyolitic ignimbrite.

Keywords Delanta opal · Gemstone · Wegel Tena · Volcanic-hosted · Ignimbrite · Geochemistry · Ethiopia

Introduction

A gemstone or gem, also called a precious or semi-precious stone, is a piece of attractive mineral used to make jewelry or other adornments (Zewdie et al. 2009). Opal, aquamarine, emerald, peridot, garnet, spinel, tourmaline, topaz, corundum, and etc. are some of the minerals used as a gem (Fritsch and Rondeau 2009). Most gemstones are hard, but some soft minerals or non-crystalline materials of organic origin (e.g., pearl, red coral, and amber) are used in jewelry because of their luster or other physical properties with esthetic value. Rarity is another characteristic that adds value to a gemstone.

Opal is one of the gemstones (chemical formula $SiO_2 \cdot nH_2O$) corresponding to a hydrated, amorphous, or poorly crystallized silica (Jone and Segnit 1971; Elzea and Rice 1996; Yu 2009; Wilson 2014; Curtis et al. 2019; Fröhlich 2020). Its water content can vary from 3 to 18 wt % (Langer and Flörke 1974; Aguilar-Reyes 2004). The microstructure within the opal is mainly responsible for the play of color. Accordingly, the opal is classified into opal-C (well-ordered α-cristobalite), opal-CT (disordered α-cristobalite and α-tridymite), and opal-A (highly disordered, nearly amorphous) structural groups (Jones and Segnit 1971; Guthrie et al. 1995; Elzea and Rice 1996; Smallwood et al. 1997; Langer and Flörke 1974); furthermore, Langer and Flörke (1974) subdivided opal-A into opal-AN (amorphous opal with a glass-like structure) and opal-AG (aggregated spheres of amorphous silica). Apart from the structural grouping of the opal, geochemical characteristics are also used to identify the geographical origin of the gem material

Responsible Editor: Domenico M. Doronzo

✉ Daniel Meshesha
daniel.meshesha@aastu.edu.et

1 Department of Geology, College of Applied Science, Addis Ababa Science and Technology University, P.O. Box 16417, Addis Ababa, Ethiopia

2 Mineral Exploration, Extraction and Processing Centre of Excellence, Addis Ababa Science and Technology University, P.O. Box 16417, Addis Ababa, Ethiopia

under consideration (e.g., Abduriyim et al. 2006; Peucat et al. 2007; Rossman 2009). Common opal is widespread, whereas precious opal occurs in some countries, such as Brazil, Mexico, Australia, Honduras, Guatemala, USA, Peru, Indonesia, Poland, Slovakia, Canada, New Zealand, Tanzania, Zambia, and Ethiopia (e.g., Koivula et al. 1983; Shigley et al. 2009; Ansori 2010; Simoni et al. 2010; Caucia et al. 2013; Chauviré et al. 2017). There are many types of precious opal (black, fire (intense red), boulder (attached to the host rock), blue, and pink) found around the world. They are associated with sedimentary and volcanic environments (e.g., Gallacher 2001). For instance, Mexican and Ethiopian opals are of volcanic origin, while Brazilian and Australian opals are of sedimentary origin. Australian, USA, and Mexican opals are the most valuable opals in the world.

Opal is precipitated from an SiO_2-enriched solution in cavities that resulted from the weathering of volcanic (rhyolite; e.g., Mexico and Ethiopia) or sedimentary (sandstone; e.g., Australia and Brazil) rocks (Koivula et al. 1983; Gübelin 1986; Bartoli et al. 1990; McOrist et al. 1994; Johnson et al. 1996; Eckert 1997; Dowell et al. 2002; Gaillou et al. 2008; Zewdie et al. 2009; Rondeau et al. 2012; Rey 2013; Dutkiewicz et al. 2015; Kiefert et al. 2014; Chauviré et al. 2017, 2019). Generally, three main processes have been identified for the origin of opal mineralization: biological precipitation (Clarke 2003; Liang et al. 2020), hydrothermal alteration (Goryniuk et al. 2004; Barnes et al. 2009; Campbell et al. 2015), and continental weathering (Thiry and Simon-Coinçon 1996; Ullyott et al. 2004; Thiry et al. 2006). Chauviré et al. (2017) suggested that opals from Wegel Tena are of pedogenetic origin and related to continental weathering. The continental weathering dissolves primary minerals and releases silica available for opal formation (Thiry and Simon-Coinçon 1996). Biogenic silica is a form of biologically produced silicon dioxide ($SiO_2{\cdot}nH_2O$) secreted as skeletal material by pelagic phytoplankton (diatoms) and one group of pelagic zooplankton (radiolarians) accumulating in oceanic or lacustrine sediments (Iler 1979). Hydrothermal alteration is involved in amorphous silica precipitation in hot springs (e.g., geysers) and hydrothermal vents (e.g., black smokers) (Jones and Renaut 2004; Lynne et al. 2005; Rodgers et al. 2004). Hydrothermal alteration occurs from 50 to 500 °C while weathering occurs below 50 °C (Pirajno 2009). Continental weathering of rocks also dissolves primary minerals and releases silica, which is then available for forming secondary minerals, including opal (Rondeau et al. 2012; Liesegang and Milke 2014; Chauviré et al. 2017, 2019).

In Ethiopia, opal occurs in Mezezo, Shewa Province (Rondeau et al. 2010, 2012), and Wegel Tena in the northeast of Wollo Province (Johnson et al. 1996; Gauthier et al. 2004). Delanta opal in the Wegel Tena area occurs in weathered rhyolitic ignimbrite of a thick volcanic sequence (Rondeau et al. 2010, 2012; Chauviré et al. 2017, 2019). It is primarily white, with some brown opal, fire opal, and colorless "crystal" opal (Mazzero et al. 2009; Rondeau et al. 2010), which resemble Australian and Brazilian opals because of their intense play of color (Rondeau et al. 2010). However, the geochemical relationship between the host rhyolitic ignimbrite and opal mineralization is not well constrained.

The region around the study area consists of a thick (> 3000 m) volcanic sequence of flood basalts and an overlying sequence of alternating layers of rhyolitic ignimbrites (Rondeau et al. 2010, 2012; Chauviré et al. 2017, 2019) and basalts (Ayalew and Yirgu 2003). The layers of basalt range from a few meters to hundreds of meters thick, whereas the thickness of ignimbrite locally reaches up to 700 m (Ayalew and Yirgu 2003). The entire sequence in the study area forms a plateau with a surface area of 1600 km^2 that is part of a larger Oligocene volcanic province.

Therefore, our new data set from the Delanta area has been used to investigate the geology and the geochemical relationship between opal and the host rock. The samples studied in this article were collected from Berbere Wonz, Koke Wuha, and Tantakoa area for a better understanding of opal formation in this area.

Geological setting

The East African Rift System (EARS) is one of the largest and currently active igneous provinces in East Africa. It is characterized by a 2000 km long and widely distributed volcanic province as a result of lithospheric extension due to the domal uplift of the surrounding regions (e.g., Kieffer et al. 2004; Wolfenden et al. 2004). Distribution and timing of magmatism and uplift in EARS is the result of an upwelling of an anomalously hot mantle plume (e.g., Berhe et al. 1987; Ebinger and Sleep 1998).

The uplifted Ethiopian plateau is bisected by NNE-SSW running Ethiopian rift system for about a distance of 1000 km. The rift system is connected with the Red Sea and Gulf of Aden oceanic spreading centers through the Afar triple junction (Merla et al. 1979; Baker et al. 2000). Before the African-Arabian continental break-up, the pre-rift volcanic activity was initiated by the arrival of a mantle plume. It piled up a large volume of basaltic lavas that formed the Ethiopian and Yemen plateaus (Beccaluva et al. 2009). The magmatic activity started between 45 and 35 Ma in southern Ethiopia and was followed by the Oligocene continental flood basalts erupted between 31 and 28 Ma in the northwestern Ethiopian plateau (Berhe et al. 1987; Ebinger et al. 1993; George et al. 1998). In the Ethiopian plateau, about 350,000 km^3 of Oligocene continental flood basalts erupted within a short period of time (Hofmann et al. 1997; Pik et al. 1998; Ukstins et al. 2002; Meshesha and Shinjo 2007;

Beccaluva et al. 2009). Pik et al. (1998, 1999) geochemically subdivided the continental flood basalt of the northwestern Ethiopian Plateau into low-Ti (LT-type) and high-Ti (HT1 and HT2 type) basalts. Compositionally, LT and HT1 types are tholeiitic, whereas HT2 type is transitional (Beccaluva et al. 2009; Natali et al. 2016). Following the cessation of the fissural-type Oligocene magmatic activity, the build-up of shield volcanoes started (e.g., ~ 30 Ma Simien Shield (Coulie et al. 2003); 23 Ma Choke and Guguftu Shield (Kieffer et al. 2004); 11.2–7.8 Ma Wollega shield volcano (Berhe et al. 1987)). Compositionally, the shield volcanoes are bimodal.

The investigated area is situated within the northwestern plateau of Ethiopia (Fig. 1A). It is located in the south Wollo zone, Delanta woreda. It is about 550 km north of Addis Ababa and 110 km NW of Dessie and referred to as "Delanta," which corresponds to a former subdivision (or "awraja") of the Wollo zone (Rondeau et al. 2010). The region contains a large deposit of opal around the Wegel Tena and Tsehay Mewcha localities.

Over the entire volcanic sequence, only the weathered rhyolitic ignimbrite is mineralized with opal (Figs. 1B and 2) (Rondeau et al. 2010, 2012; Chauviré et al. 2017). The mineralized layers (< 1 m thick) are sandwiched between thick and welded rhyolitic ignimbrites dated at 29.8 Ma (Ayalew et al. 2002). Common opal and opal with play of color opal most often cement grains of volcanic debris or sometimes fill in fractures or cavities in the rock. As a result, the rough gem material often has an irregular shape (Rondeau et al. 2010, 2012; Chauviré et al. 2017, 2019). During the fieldwork, in the three investigated mines (Berbere Wonz and Koke Wuha (Wegel Tena area); Tantakoa (Tsehay Mewcha area)), gem opal occurs in one lenticular opal-bearing horizon within the unwelded and weathered rhyolitic ignimbrite bed which is composed of brownish, clayey, and soft friable rock (Fig. 1B). These mines are all located on the steep sides of the plateau. The horizon is highly weathered, containing altered volcanic glass, a granular microstructure cemented by opal, and cavities filled with clay. The cliff-forming unweathered, thick and highly welded rhyolitic ignimbrite that overlies the opal-bearing unit is an impermeable medium, preventing later percolation of fluids (Chauviré et al. 2019), and it acts as a barrier for storing certain amounts of water and silica solution below (Fig. 1B).

Sampling and analytical techniques

Thirty rhyolitic ignimbrite rock samples were sent to the Geoscience Central Laboratory of the Ethiopian Geological Survey for thin section preparation. The petrographic examination was done for the host rock of opal. The thin sections were examined using a petrographic microscope (Leica DM750 with camera) in the petrology laboratory of the Department of Geology, Addis Ababa Science and Technology University (AASTU). Thirteen (10 rhyolitic ignimbrites and 3 opals) samples were selected for major and trace element analysis (Tables 1 and 2). Samples were prepared for whole-rock geochemical analysis in Australia Laboratory Services (ALS) in Addis Ababa, Ethiopia. To determine the geochemical composition, the samples were crushed into chips with 70% of the crushed samples being less than 2 mm in size and further pulverized up to 250 g

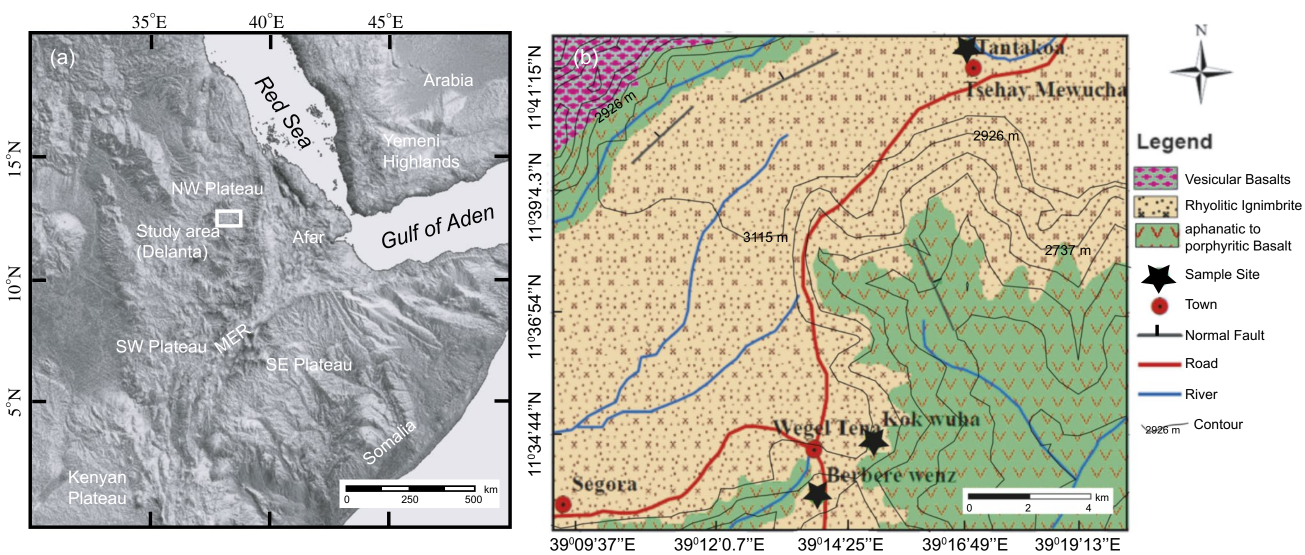

Fig. 1 Location map of the study area. **a** Shaded relief map of NW Africa and Arabia (NASA SRTM30) showing the position of the three rifts (Main Ethiopian Rift, MER; Gulf of Aden; Red Sea) as well as the Ethiopian and Yemeni plateaus with the location of Delanta area. **b** Simplified geological map of the Delanta area

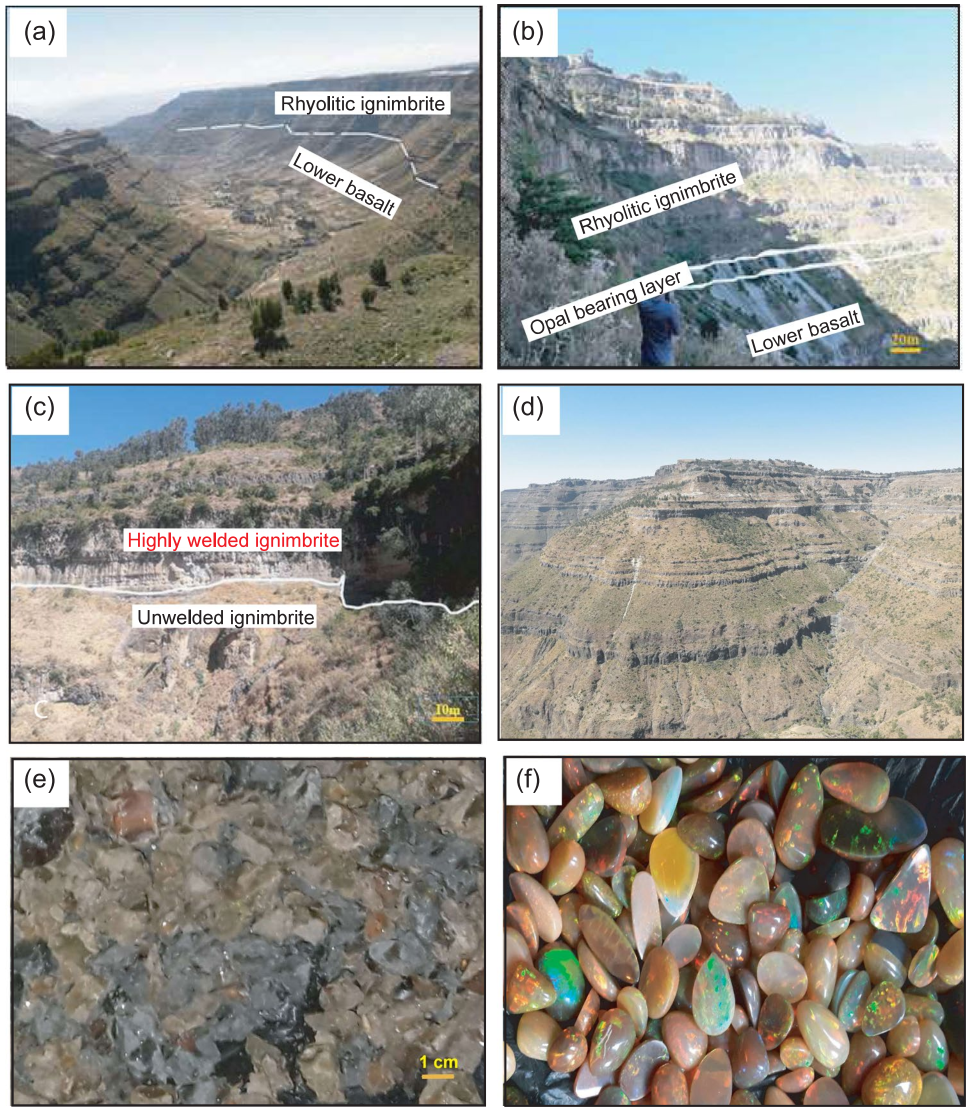

Fig. 2 General lithostratigraphy of the study area. **a** Different lithologies and layers of the volcanic sequence. **b** The lower basalt below the opal-bearing layer, and the upper parts of the rhyolitic ignimbrite forms steep cliff with an alternating layer of both welded and unwelded, and at the middle a very thin layer, not more than 1 m thick of opal-bearing horizon. **c** The variation of topographic slopes, the top part steep slope cliff is formed by highly welded ignimbrite, and lower part relatively gentle slope topography is formed by unwelded ignimbrite. **d** A typical viewpoint of rhyolite ignimbrite layers. **e** Grains of opal collected by local people. **f** A photo of play of color opals mined at Wegel Tena

of sample with 85% of the samples passing through 75-µm mesh. The pulverized samples weighing 0.7 kg were sent to Ireland and processed at ALS Loughrea, Ireland.

Samples are decomposed using lithium metaborate/lithium tetraborate fusion. A prepared sample (0.2 g) is added to lithium metaborate/lithium tetraborate flux (0.90 g), mixed well, and fused at 1000 °C. The resulting melt is then cooled and dissolved in 100 mL of 4% HNO_3 and 2% HCl. This solution is then analyzed by inductively coupled plasma atomic emission spectroscopy (ICP-AES) and the results are corrected for spectral inter-element interferences. Oxide concentration is calculated from the determined elemental concentrations. The total oxide content is determined from the ICP analytic concentrations and loss on ignition (LOI) values. For LOI determination, a sample weighing 0.1 g is placed in an oven at 1000 °C for 1 h, cooled, and weighed. The percent on loss ignition is then calculated from the difference in weight.

For ultra-trace elements, the samples are decomposed using lithium metaborate fusion (FUS-LI01). Accordingly, a sample of 0.2 g is added to lithium metaborate flux (0.90 g), mixed well, and fused in a furnace at 1000 °C. The resulting melt is then cooled and dissolved in 100 mL of 4% HNO_3/2% HCl. This solution is then analyzed by inductively coupled plasma-mass spectrometry (ICP-MS, Agilent 7700 Technology). The detection limits of all trace elements are presented in Table 3. Reproducibility and accuracy were checked using blank (< 1%) and international rock standards (REE-1 and SY-4).

Petrography of rhyolitic ignimbrite

The samples were taken from the opal mine tunnels (Table 1). The petrographic examination result shows similar petrography at all investigated sites (Berbere Wonz, Koke

Table 1 Summary of rhyolitic ignimbrite description from Delanta area

No	Sample	Locality	Field descriptions	Petrographic description (% modal proportion)								Geochemical analysis	
				Volcanic glass	Quartz	Plagioclase	Biotite	Opaque	Hornblende	Sanidine	Lithic fragment	Major and trace element	Opal sample (only trace element)
1	TAT-100A	Tantakoa	Rhyolitic Ignimbrite: dark gray, aphanitic, unwelded. Set in gentle slope	80	9	6	2	2			1	√	OTAT-01
2	TAT-100B		Rhyolitic Ignimbrite: light gray, aphanitic, unwelded. Set in gentle slope	80	8	6	2	3			1	√	
3	TAT-100C		Rhyolitic Ignimbrite: dark and light gray is common, aphanitic, unwelded. Set in gentle slope	82	8	6	1	1		1	1	√	
4	TAT-101B		Rhyolitic Ignimbrite: light gray, aphanitic, highly welded. Set in gentle slope	80	8	6	2	1		2	1		
5	KOW-200A	Koke Wuha	Rhyolitic Ignimbrite: light gray, aphanitic with rock fragment, slightly welded	85	7	3	1	1		2	1		OKOW-01
6	KOW-200B		Rhyolitic Ignimbrite: light gray, aphanitic with rock fragment, welded	82	7	4	2		2	2	1	√	
7	KOW-200C		Rhyolitic Ignimbrite: light gray, aphanitic, moderately welded	85	6	6	1	1			1	√	
8	KOW-200D		Rhyolitic Ignimbrite: light gray, aphanitic, moderately welded	86	4	7	1	1			1	√	
9	BEW-300A	Berbere Wenz	Rhyolitic Ignimbrite: light to dark gray, aphanitic with glass shards, unwelded,	80	10	4	2	1		2	1	√	OBEW-02
10	BEW-300B		Rhyolitic Ignimbrite: light gray, aphanitic with glass shards, unwelded	78	10	6	2	1		2	1	√	
11	BEW-300C		Rhyolitic Ignimbrite: dark gray, aphanitic with rock fragments, slightly welded	80	9	6	2			2	1	√	
12	BEW-300D		Rhyolitic Ignimbrite: light gray, aphanitic with rock fragment, unwelded	78	10	7	2			2	1		
13	BEW-301A		Rhyolitic Ignimbrite: light gray, fine to medium-grained with rock fragmented, highly welded	80	10	5	2			2	1	√	

Table 2 Major element (wt %) analytical results of rhyolitic ignimbrite from Delanta area

Type	Rhyolitic Ignimbrite									
Sample no	TAT-100A	TAT-100C	TAT-101B	KOW-200B	KOW-200C	KOW-200D	BEW-300A	BEW-300B	BEW-300C	BEW-301A
Easting (m)	529,172	529,172	529,123	525,552	525,552	525,552	523,966	523,966	523,966	523,948
Northing (m)	1,293,271	1E+06	1,293,261	1,281,697	1,281,697	1,281,697	1,278,623	1E+06	1E+06	1,278,716
SiO_2	57.80	56.80	58.70	59.50	59.80	59.90	58.60	56.60	56.20	64.60
Al_2O_3	13.25	13.75	13.5	13.45	14.00	13.75	14.2	14.5	14.05	13.25
Fe_2O_3	6.52	6.77	6.82	6.53	6.46	6.56	6.88	6.77	8.01	4.90
CaO	1.84	1.83	2.68	1.47	1.32	1.23	1.48	1.58	2.37	1.10
MgO	0.93	1.07	1.03	0.79	0.89	0.73	0.70	0.74	1.21	0.63
Na_2O	1.25	1.17	1.39	1.76	2.07	2.08	1.50	1.27	2.11	1.83
K_2O	1.55	1.39	1.75	1.94	1.74	1.85	1.75	1.53	1.44	2.72
TiO_2	1.60	1.66	1.58	1.05	1.06	1.03	1.10	1.10	1.53	0.64
MnO	0.11	0.12	0.13	0.21	0.20	0.19	0.35	0.43	0.33	0.15
P_2O_5	0.08	0.08	0.52	0.09	0.11	0.11	0.05	0.05	0.23	0.01
LOI	14.40	14.85	13.05	13.15	11.8	12.1	13.65	14.55	11.9	10.65
Total	99.41	99.55	101.30	99.97	99.48	99.56	100.00	99.17	99.44	100.30

TAT samples from Tantakoa, *KOW* samples from Koke Wuha, *BEW* samples from Berbere Wonz

Table 3 Trace element content (ppm) of rhyolitic ignimbrite and opal from Delanta area

Type	Rhyolitic ignimbrite										Opal			
Sample	TAT-100A	TAT-100C	TAT-101B	KOW-200B	KOW-200C	KOW-200D	BEW-300A	BEW-300B	BEW-300C	BEW-301A	OTAT-01	OKOW-01	OBEW-02	DL
Ba	598	482	511	320	293	293	366	450	403	486	18.4	19.13	31.79	0.5
Cr	20	20	20	10	10	10	10	10	20	10	nd	nd	nd	10
Cs	2.63	2.36	2.52	3.76	3.62	3.63	3.84	3.21	2.25	2.34	0.27	0.22	0.53	0.01
Ga	30.2	31	29.4	36.4	39.6	39.2	42.8	42.6	40	32.7	nd	nd	nd	0.1
Hf	14.1	15.8	14.1	33.0	35.7	36.9	35.2	37.7	31.6	13.7	2.1	1.9	2	0.1
Nb	71.2	80.3	71.2	160	174	177	171.5	183.5	161.5	62.7	14.82	21.49	2.05	0.1
Rb	67.7	60.9	76	94.3	85.9	95.0	69.2	63.6	46.8	89.3	2.81	5.94	17.28	0.2
Sn	5	6	5	11	12	11	11	11	11	6	nd	nd	nd	1
Sr	219	204	265	98.8	82.4	77.1	88.6	83.7	229	78.3	10.52	13.92	70.17	0.1
Ta	4.4	4.8	4.1	10.4	11.2	10.8	10.9	11.2	9.4	3.3	nd	nd	nd	0.1
Th	9.32	10.3	9.38	23.1	24.9	25.2	24.3	26.4	21.7	10.05	2.09	0.17	0.2	0.05
U	5.03	4.44	2.44	6.32	6.39	6.45	5.78	5.59	6.36	2.7	1.21	0.33	0.13	0.05
V	59	68	71	41	69	36	72	56	99	28	nd	nd	nd	5
Y	82.3	85	74.8	113.5	114	116	93.6	108	121	37.5	3.09	3.13	1.6	0.1
Zr	573	654	587	1380	1450	1460	1430	1540	1310	483	68.8	57.3	10.5	2
La	129.0	145.5	76.8	124.0	128.0	127.0	116.5	129.5	112.5	48.1	2.792	0.090	0.055	0.1
Ce	226	276	151.5	281	295	294	282	313	268	111.5	15.55	1.173	0.334	0.1
Pr	32.90	39.10	19.80	35.00	36.30	36.20	33.90	35.10	33.50	11.9	0.546	0.044	0.031	0.02
Nd	128	149.5	79.3	132	141.5	139.5	129.5	134.5	129	44.9	1.969	0.189	0.124	0.1
Sm	24.20	29.70	16.45	28.90	29.40	29.50	27.40	27.30	27.00	8.37	0.505	0.103	0.058	0.03
Eu	6.42	7.10	4.38	6.88	7.24	7.06	6.79	6.89	7.49	1.48	0.02	0.006	0.002	0.02
Gd	22.2	24.90	15.15	25.30	26.70	25.70	22.50	25.20	24.80	7.75	0.468	0.183	0.113	0.05
Tb	3.37	3.65	2.26	4.01	4.26	4.26	3.83	3.83	3.92	1.20	0.108	0.048	0.023	0.01
Dy	18.25	19.75	12.5	22.6	23.9	23.9	20.7	20.8	23.1	7.39	0.767	0.412	0.151	0.05
Ho	3.45	3.61	2.45	4.61	4.62	4.82	4.01	4.32	4.73	1.49	0.153	0.091	0.034	0.01
Er	8.88	9.48	7.14	12.80	13.10	12.75	10.85	11.90	13.40	4.12	0.477	0.329	0.12	0.03
Tm	1.14	1.14	0.83	1.67	1.67	1.64	1.44	1.6	1.74	0.58	0.086	0.07	0.018	0.01
Yb	7.68	7.52	5.4	11.2	11.25	11.3	8.62	10.7	11.75	4.14	0.711	0.675	0.138	0.03
Lu	0.99	1.05	0.83	1.59	1.56	1.59	1.37	1.47	1.71	0.55	0.116	0.120	0.022	0.01

nd not detected; *DL* detection limits

Wuha, and Tantakoa). The rhyolitic ignimbrite is unwelded porphyritic in texture, with common phenocrysts and microphenocrysts of quartz, plagioclase, and alkali feldspar. The phenocrysts are euhedral to subhedral in shape with some broken crystals within weathered and altered fine-grained and/or glassy groundmass; phenocrysts are also embedded in a glassy groundmass to give a vitrophric texture to the rhyolitic ignimbrite (Fig. 3). There are also minor to trace biotite, hornblende, opaque minerals, and volcanic lithic fragments (Table 1).

There are some slight variations in the opal-bearing horizon from one mine to another. At Berbere Wenz, opal cement, a highly weathered rhyolitic ignimbrite and clay material, is apparent, whereas, at Tantakoa and Koke Wuha sites, the rhyolitic ignimbrite is characterized by a smaller amount of clay (Fig. 1).

Whole-rock geochemistry

Major element data for the studied samples are presented in Table 2. The rhyolitic ignimbrite (host rock) consists of SiO_2 (56.2–64.6 wt%), Al_2O_3 (13.25–14.50 wt%), Fe_2O_3 (4.90–8.01 wt%), MgO (0.63–1.21 wt%), CaO (1.10–2.68 wt%), Na_2O (1.17–2.11 wt%), K_2O (1.39–2.72 wt%), and P_2O_5 (0.01–0.52 wt%). K_2O and Na_2O show a positive correlation with SiO_2, whereas CaO and Fe_2O_3 are negatively correlated with SiO_2. High LOI values (10.65–14.85) for most samples (Table 2) suggest that the rhyolitic ignimbrite has gone through strong alteration.

In the total Alkali-Silica (TAS) classification diagram of Le Bas et al. (1986), almost all rhyolitic ignimbrite samples fall in the dacites field (Fig. 4A) due to their significant alteration. However, on the Winchester and Floyd (1997) volcanic classification diagram using immobile elements (Nb/Y vs. $Zr/TiO_2 \times 0.0001$), all samples fall in the field of trachyte and comendites/pantellerites (Fig. 4C), except for three samples (TAT-100A, TAT-100C, and TAT-101E) that fall on the dividing line between rhyolite and trachyandesite. The variation between the two classifications is caused by the effect of alteration on Na_2O and K_2O. In addition, the chemical index of alteration ($CIA = [Al_2O_3/(Al_2O_3 + CaO* + Na_2O + K_2O)]100$; Nesbitt and Young 1982) and Chemical Index of Weathering ($CIW = [Al_2O_3/(Al_2O_3 + CaO* + Na_2O)]100$; Harnois 1988) are used to quantify the degree of weathering to which rocks have been subjected. Hence, as shown in Fig. 4B, the calculated values of CIA (70–75) and CIW (76–84) suggest intermediate to extreme silicate weathering.

Trace element data for the studied samples are presented in Table 3. The rhyolitic ignimbrite shows higher values in trace elements such as Zr (483–1540 ppm), Rb (47–95 ppm), Y (38–121 ppm), Nd (45–150 ppm), Nb (63–184 ppm), Ba

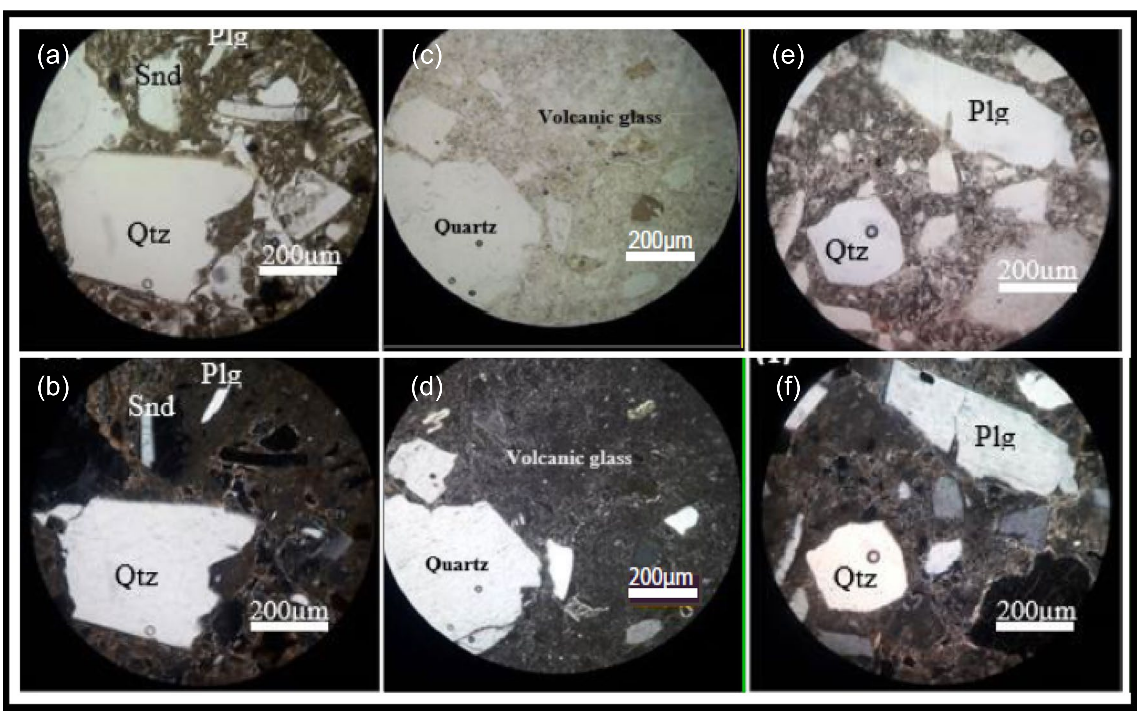

Fig. 3 Microphotograph of TAT-101B. **a** PPL and **b** XPL; KOW-200D. **c** PPL and **d** XPL; BEW-300D. **e** PPL and **f** XPL. Plg = plagioclase, Qtz = quartz, Snd = sanidine, Rft = rock fragment, and Opq = opaque mineral. The phenocrysts are anhedral and the groundmass is dominated by brownish to light gray volcanic glass

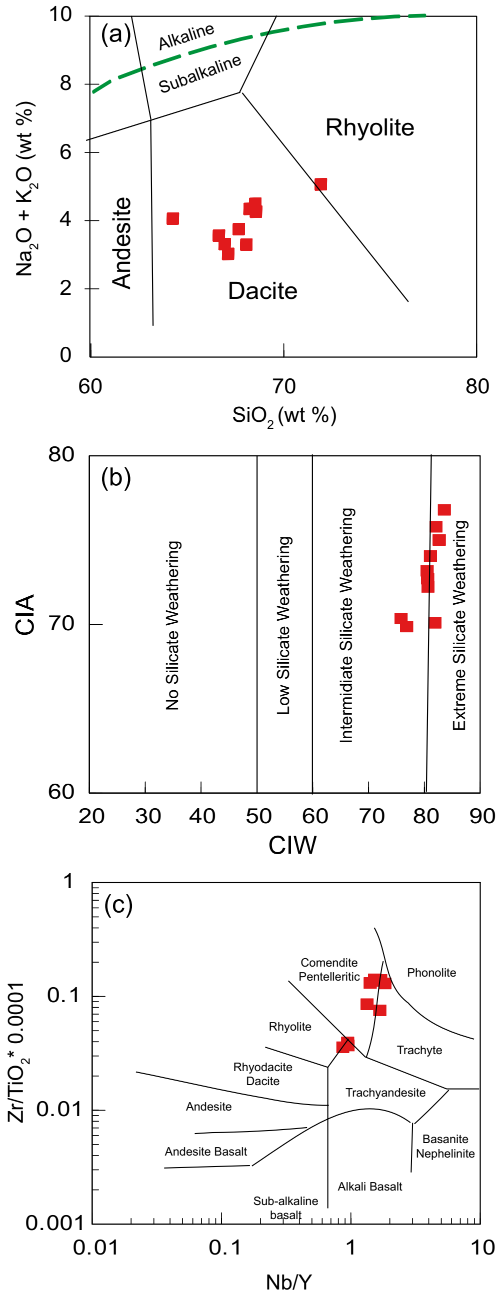

Fig. 4 **A** Total alkali-silica (Na_2O+K_2O) versus SiO_2 diagram (Le Bas et al. 1986). **b** Chemical Index of Weathering (CIW = [Al_2O_3/(Al_2O_3 + CaO + Na_2O)]*100; Harnois 1988) versus alteration (CIA = [Al_2O_3/(Al_2O_3 + CaO + K_2O + Na_2O)]*100; Nesbitt and Young 1982). **c** Nb/Y vs. Zr/TiO_2 *0.0001 diagram (Winchester and Floyd 1997) of rhyolitic ignimbrite

(293–598 ppm), La (48–130 ppm), Sr (77–265 ppm), and Ce (112–313 ppm).

All host rock samples show nearly typical patterns for rhyolite in the primitive mantle normalized multi-element diagram (Fig. 5A). All trace elements in this diagram are enriched relative to the primitive mantle and display marked depletion in Ba, K, Sr, P, and Ti which are possibly the consequence of fractionation of alkali feldspar (Ba and K), plagioclase feldspar (Sr), apatite (P), and Fe-Ti oxide (Ti). They show a light REE-enriched chondrite-normalized REE pattern. The analyzed rhyolitic ignimbrites are all LREE-enriched and have relatively unfractionated heavy REE (HREE) patterns (Fig. 5B; $(La/Lu)_N = 7.05–14.65$; $(La/Sm)_N = 2.68–3.70$; $(Gd/Yb)_N = 1.55–2.74$). In general, very weak (for sample BEW-301A) or absent Eu anomalies were observed in the host rock.

Trace element values in opal samples are Zr (10.5–68.8 ppm), Ba (18.40–31.79 ppm), Nb (2.05–21.49 ppm), Ce (0.334–15.55 ppm), Sr (10.52–70.17 ppm), and Rb (2.81–17.28 ppm). The opal samples show variable LREE to almost homogenous HREE, Eu negative anomaly (Eu/Eu* = 0.08–0.13) and generally positive Ce anomaly (Ce/Ce* = 2.2–3) (Fig. 5B; $(La/Lu)_N = 0.08–2.63$; $(La/Sm)_N = 0.57–3.65$; $(Gd/Yb)_N = 0.22–0.68$). Generally, the opal samples are characterized by slightly negative slopes for LREE, relatively flat HREE patterns, pronounced negative Eu anomalies, and positive Ce anomalies.

The three opal host rock pairs are characterized by slight enrichment in LREE than HREE (Fig. 5B). However, a progressive increase is observed in opal from Gd to Lu compared to the host rock. Their difference is in the variation of trace element and REE concentrations between opal and its host rock. It has always a lower elemental concentration with pronounced negative Eu anomalies in opal compared to its host rock, which can be attributed to a dilution by weathering solutions (Gaillou et al. 2008; Ayalew et al. 2020) and/or the lower trace element concentration in opal, because it accepts less trace elements in its structure.

Discussion

The result from the petrographic examination shows similar petrography at all investigated sites. The similarity might indicate the intensity of weathering was nearly identical throughout the study area (Fig. 4b; CIW = ~80). The weathering conditions of the opal host rock suggest that the water may come from the surface or ground, or maybe rainwater, which is responsible for altering feldspar and volcanic glass from the host rock. The water from the surface and deeper levels can be of meteoric origin. According to Chauviré et al. (2019) and Ayalew et al. (2020), the oxygen isotope of the opal samples from the Wegel Tena ($\delta^{18}O = 26.52–30.98$ ‰) and Mezezo ($\delta^{18}O = 28.4–33.8\%$) area indicates that weakly evaporated soil water fed by meteoric water is responsible for the opal formation at low temperature between 18 and 21 °C for Wegel Tena and between 21 and 26 °C for Mezezo area. The high oxygen isotope ($\delta^{18}O$) values and low

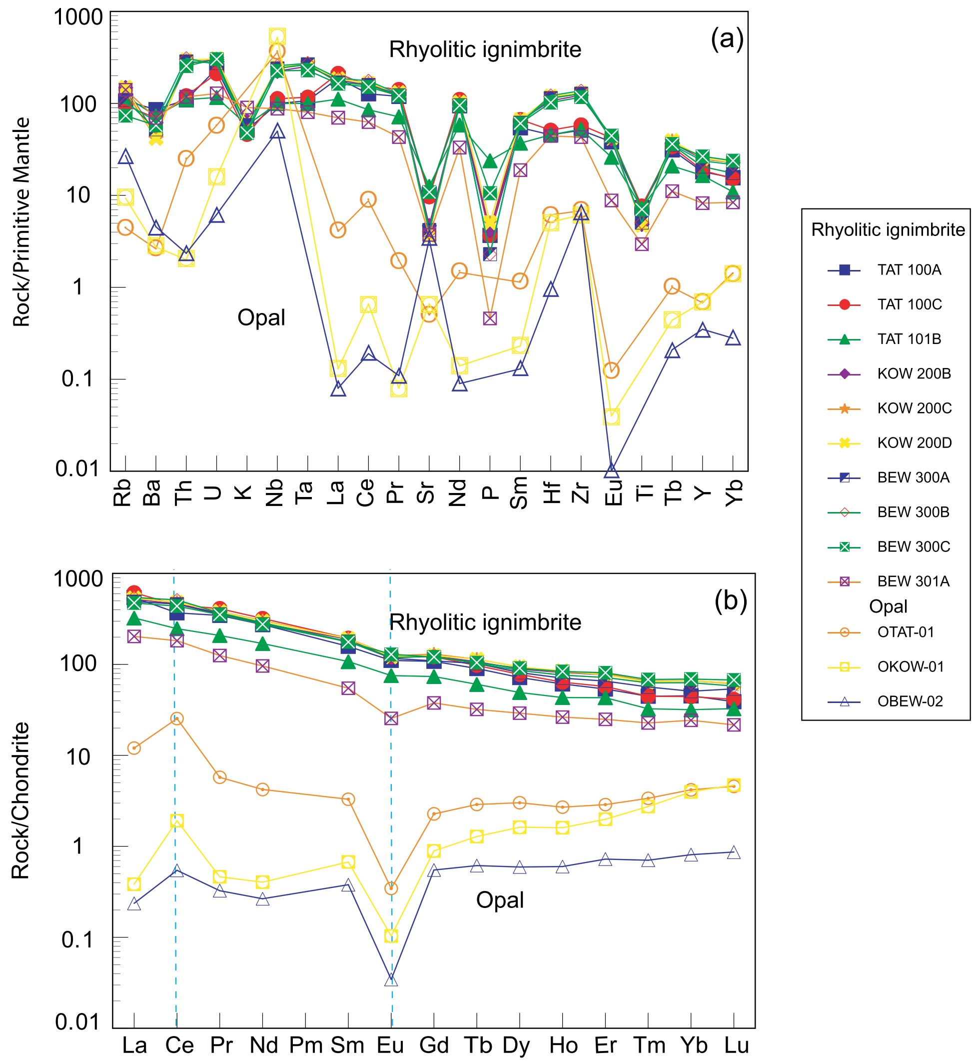

Fig. 5 **A** Multi-element and **b** REE diagram of Delanta opal and host rock normalized to primitive mantle and chondrite respectively. Normalization values are taken from Sun and McDonough (1989)

temperature indicate a pedogenetic origin of both Wegel Tena (Chauviré et al. 2017) and Mezezo area (Ayalew et al. 2020), whereas the oxygen isotope of unweathered rhyolite from Wegel Tena ranges from 5.8 to 7‰ (Ayalew et al. 2002). Similarly, Martin and Gaillou (2018) discussed a similar process using oxygen ($\delta^{18}O = \sim 30‰$) and hydrogen isotopes where the opal from Tecopia (California, USA) is precipitated from groundwater due to an evaporation mechanism. Rondeau et al. (2004) also reported a high oxygen isotope ($\delta^{18}O = \sim 31$ ‰) for Slovakian and Australian opals with formation temperature lower than 45 °C. The weakly evaporated soil water solution creates a favorable condition for the precipitation of opal in primary or secondary openings like cracks, voids, and veins, which are caused by natural faults and fractures.

Rhyolitic ignimbrite and opal samples in the study area show variable geochemical characteristics where the opal exhibits depleted trace element concentrations compared to the host rock. The presence and concentration of trace elements in opals reflect variations from the host rock composition, as silica in opal comes from its alteration (Rondeau et al. 2012; Chauviré et al. 2019). The Chemical Index of Alteration (CIA, Fig. 4B) also indicates that the dominant process during chemical weathering is the degradation of feldspar and volcanic glass for forming clay minerals (Rondeau et al. 2012; Chauviré et al. 2017). In addition, some of the differences in trace elements might arise from fractionation during opal precipitation. Petrologically, the host rhyolitic ignimbrite consists of quartz, volcanic glass, plagioclase, and alkali feldspar. The alteration of them is the source of trace element variations during the weathering processes. For example, feldspar weathering releases Al^{+3}, K^{+1}, and Na^{+1} substituting Eu^{+2}, Ba^{+2}, and Sr^{+2} elements. The concentration of trace elements in opal is highly variable.

The opal samples show more depletion in trace elements than the rhyolitic ignimbrite, and still it is characterized by slight enrichment from Gd to Lu with negative Eu anomaly and positive Ce anomaly. Elsewhere in volcanic environments, opals have a negative Ce anomaly (Mexico, Gaillou et al. 2008; Ethiopia, Chauviré et al. 2019); this may indicate that during the formation of opals, conditions were oxidizing (Gaillou et al. 2008). However, the Ce anomaly was not present in the opal host rock (rhyolitic ignimbrite), indicating that the weathering of the host rock is responsible for the Ce anomaly (Gaillou et al. 2008; Rondeau et al. 2012; Chauviré et al. 2019) at extremely oxidizing conditions. Ce and Eu can exist in the valence states Ce^{+4} and Eu^{+2}, respectively, because of the unique electron arrangement in their outer shell differ from other REE. The change from Eu^{+3} to Eu^{+2}, which is a reducing condition, is indicated by the negative anomaly of Eu, whereas the change from Ce^{+3} to Ce^{+4}, which is an oxidizing situation, is indicated by the positive anomaly of Ce. A slight enrichment of LREE compared to HREE is observed in the chondrite-normalized REE patterns of most opal samples (Fig. 5). In addition, the lack of an Eu anomaly in the host rock indicates the absence of plagioclase or alkali feldspar fractionation in the magmas that formed the host rock. The possible redox scenario that might occur is that Eu, which is primarily hosted in alkali feldspar and plagioclase, either was not leached at all or was leached more intensively than the other REE, resulting in its dispersion in the solution. The Si-carrying solution was thus already Eu-depleted, and resulted in a negative Eu anomaly. Then, under oxidizing conditions, Ce was changed from Ce^{3+} to Ce^{4+}, which made it less mobile and resulted in a positive Ce anomaly.

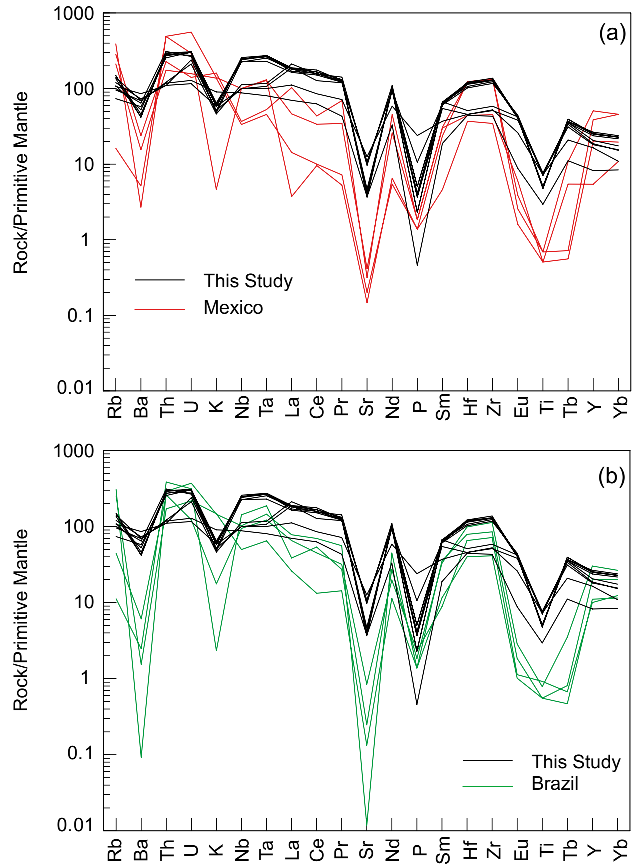

Fig. 6 Multi-element diagram of **a** Delanta/Mexico; **b** Delanta/Brazilian opal host rocks normalized to primitive mantle. Normalization values are taken from Sun and McDonough (1989)

Comparison with other opal deposits

For comparison, the volcanic environment is represented by Mexican (Durango and Olimpia) opal samples, whereas the sedimentary environment is represented by Brazilian (Para, Rio Grande do Sul, and Piaui) opal samples. The host rocks from Mexico are rhyolites or rhyolitic tuffs, and the host rocks from Brazil are sandstones. Data (major and trace element value) for Mexican and Brazilian samples are from Gaillou et al. (2008).

The host rock multi-element diagrams from volcanic and sedimentary environments show nearly similar patterns (Fig. 6A and B). All host rocks from Delanta/Mexico display typical patterns for rhyolite. The patterns have Ba, K, Sr, P, and Ti negative anomalies in Delanta/Ethiopia and they have Ba, K (two samples), Sr, P, Zr, Ti, and Eu negative anomalies in Mexican host rocks (Fig. 6A), which represent the results of magmatic differentiation. The multi-element diagram of the Brazilian host rocks has a parallel pattern with Delanta/Ethiopia showing depleted Ba, K, Sr, P, Eu, Ti, and Tb (Fig. 6B). But both Mexican and Brazilian host rocks show more Ba, K, Sr, P, Eu, Ti, and Tb depletion than Delanta/Ethiopia.

REE patterns of Delanta/Mexican host rocks show variable characteristics. Delanta rhyolitic ignimbrite shows an REE pattern with slight enrichment in LREE compared to HREE. In general, a very weak (for sample BEW-301A) or absent Eu anomaly is observed. As shown in Fig. 7, the Mexican and Brazilian host rocks exhibited depleted LREE and variable HREE with a stronger negative Eu anomaly than Delanta REE patterns.

Furthermore, REE diagram of opals from volcanic and sedimentary environments shows significant differences. Figure 8 presents typical examples of volcanic-derived opals from Delanta compared to volcanic and sedimentary ones from Mexico and Brazil, respectively. The REE patterns of Delanta (this study) and Mexico (Gaillou et al. 2008) volcanic opals show the typical negative Eu anomaly (Fig. 8A-C). A positive Ce anomaly is present in Delanta opal REE patterns (Fig. 8A); such anomalies depend on the oxidation conditions (Gaillou et al. 2008). The positive Ce anomaly is not present in the host rock (Fig. 5B), which means the positive Ce anomaly is developed during weathering of the

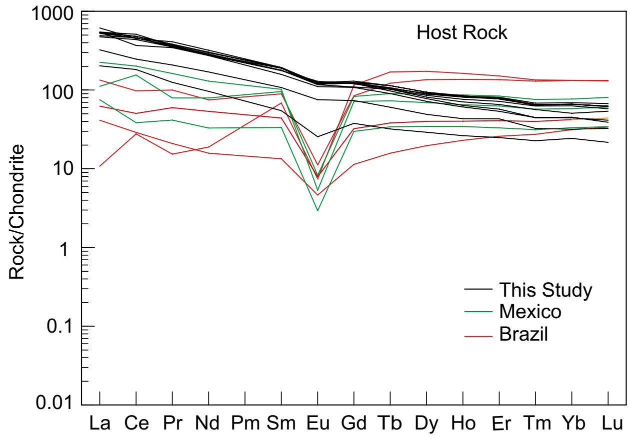

Fig. 7 Chondrite-normalized rare earth element diagrams for opal host rock samples of Delanta, Mexico, and Brazil. Normalization values are taken from Sun and McDonough (1989)

host rock. As shown in Fig. 8D, the REE patterns of Brazil sedimentary opals are characterized by a lack of pronounced Eu and Ce anomalies (Fig. 8D). According to the aforementioned discussions, geochemical data by themselves are insufficient to pinpoint the geological and geographic origin of opal. Earlier, Gaillou et al. (2008) used trace element analysis to determine the geological and geographic origin of sedimentary and volcanic opals. According to Gaillou et al. (2008), opal from volcanic rock has a lower Ba (< 110 ppm) content than that of sedimentary rock (Ba = 180–300 ppm). Later, this inference was argued by Dutkiewicz et al. (2015) and Chauviré et al. (2019), who came to the conclusion that the conditions for opal formation are specific to the local environment. However, identification of the morphological characteristics of volcanic and sedimentary opals are very important to differentiate them (Smallwood et al. 2008).

When considering the comparison of the geochemical signature of opal from various geological contexts (volcanic or sedimentary host rocks), we find that volcanic-derived opals (Delanta and Mexico) exhibit almost similar chondrite-normalized REE patterns except the Ce anomaly (Fig. 8A and C). The similarity in REE patterns may indicate that similar processes control trace element incorporation during opal precipitation (Gaillou et al. 2008; Rondeau et al. 2012). A significant variation in some elements are seen between volcanic and sedimentary-derived opals (Fig. 8 A-D). The variations may suggest that the degree of weathering, composition of source materials, and controlling factor of trace element incorporation are different. Apart from the degree of weathering and the composition of source materials, the composition of opal precipitation is strongly affected by the physical conditions of the regional and/or local environment (Chauviré et al. 2019).

Conclusion

South Wollo, Delanta opal is a recent discovery in Ethiopia and active in mining, which is mainly located around Wegel Tena and Tsehay Mewucha locality. It has great importance in the country's economy and is now sold as raw materials or cabochon cut in the gemstone markets.

The presence and concentration of trace elements in opals reflect the host rock composition primarily, as silica in opal comes from its alteration. In addition, some of the differences in chemical properties might arise from fractionation during opal precipitation.

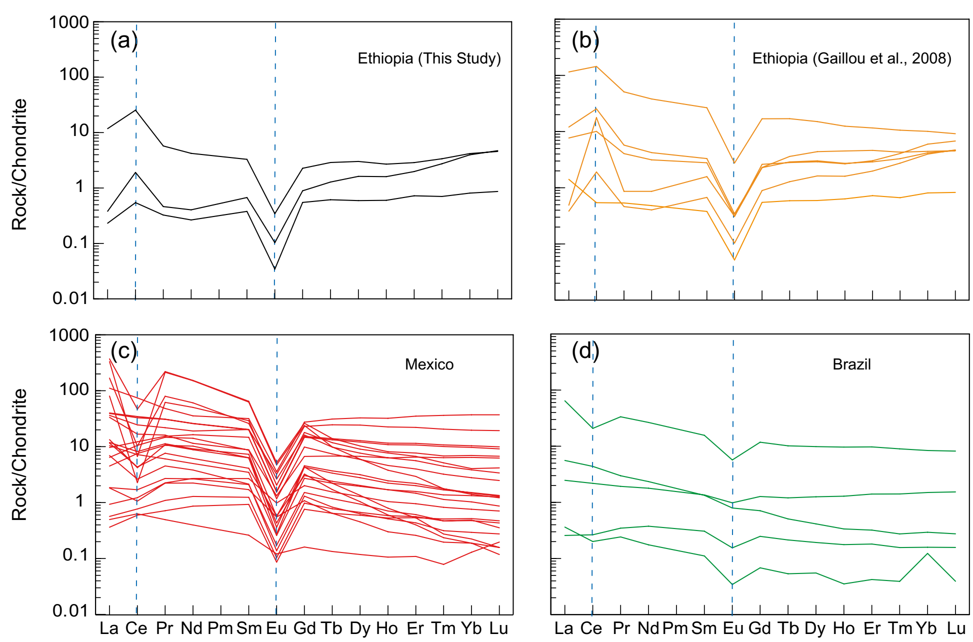

Fig. 8 Chondrite-normalized rare earth element diagram for this study Ethiopian **a**; previous study Ethiopian **b**; Mexican **c**; and Brazilian **d**; opal samples. Normalization values are taken from Sun and McDonough (1989)

Elsewhere in volcanic environments, opals have negative to slightly positive Ce anomaly, but Delanta opal from this study is characterized by a strong positive Ce anomaly. Ce anomaly may indicate that during the formation of opals, conditions were oxidizing. However, the Ce anomaly was not present in the opal host rock, suggesting that it developed during weathering. Interestingly, an absent Eu anomaly is observed in the host rock. This may be explained by the lack of plagioclase or alkali feldspar fractionation in the source.

Our investigation, based on field observation, petrographic and geochemical analysis, show a strongly weathered opal-bearing horizon with the presence of abundant clays, altered volcanic glass, high LOI values, CIA index (70–75), absence of hot springs, and geysers. These features strongly suggest that the studied opals formed from percolated meteoric water during an episode of weathering of the host rhyolitic ignimbrite.

When comparing the geochemical signature of opal from volcanic or sedimentary host rocks, we find that volcanic opals from Ethiopia show a fairly good correlation with Mexican opal. The correlation may indicate similar processes control the trace element incorporation during opal precipitation. Significant variation in Ce anomaly is seen between Ethiopian volcanic, Mexican volcanic, and Brazilian sedimentary opals. The variation in Ce anomaly may suggest that fluid chemistry is the controlling factor of trace element incorporation.

Acknowledgements MM is highly grateful to Addis Ababa Science and Technology University (AASTU) for MSc program opportunity. This work is completed due to the kind and welcoming community of Dessie, Wegel Tena, and Tsehay Mewucha. Therefore, we greatly thank those community and government officials for their cooperation and hospitality. Finally, the authors thank the anonymous reviewers and associate editor for their constructive and detailed comments that improved the manuscript.

Author contribution All authors equally contributed for the manuscript. All authors have read and agreed to the published version of the manuscript.

Data Availability Data availability is on request.

Declarations

Informed consent statement Not applicable.

Conflict of interest The authors declare no competing interests.

References

Abduriyim A, Kitawaki H, Furuya M, Schwarz D (2006) “Paraíba”-type copper-bearing tourmaline from Brazil, Nigeria and Mozambique: chemical fingerprinting by LA-ICP-MS. Gems Gemol 42:4–21

Aguilar-Reyes BO (2004) Microstructural study of opal: application to the destabilization by whitening. PhD dissertation, University of Nantes, Nantes, France, pp 174

Ansori C (2010) Model mineralisasi pembentukan opal banten. Jurnal Geol Indones 5:151–170

Ayalew D, Yirgu G (2003) Crustal contribution to the genesis of Ethiopian plateau rhyolitic ignimbrites: basalt and rhyolite geochemical provinciality. J Geol Soc London 160:47–56. https://doi.org/10.1144/0016-764901-169

Ayalew D, Barbey P, Marty B, Reisberg L, Yirgu G, Pik R (2002) Source, genesis, and timing of giant ignimbrite deposits associated with Ethiopian continental flood basalts. Geochem Cosmochim Acta 66:1429–1448. https://doi.org/10.1016/S0016-7037(01)00834-1

Ayalew D, Gibson S, Yirgu G, Ali S, Assefa D (2020) Pedogenic origin of Mezezo opal hosted in Ethiopian Miocene rhyolites. Can Mineral 58:231–246. https://doi.org/10.3749/canmin.1900059

Baker J, MacPherson CG, Menzies MA, Thirlwall MF, Al-Kadasi M, Mattey DP (2000) Resolving crustal and mantle contributions to continental flood volcanism, Yemen; constraints from mineral oxygen isotope data. J Petrol 41:1805–1820

Barnes JD, Paulick H, Sharp ZD, Bach W, Beaudoin G (2009) Stable isotope (δ18O, δD, δ37Cl) evidence for multiple fluid histories in mid-Atlantic abyssal peridotites (ODP Leg 209). Lithos 110:83–94. https://doi.org/10.1016/j.lithos.2008.12.004

Bartoli F, Bittencourt-Rosa D, Doirisse M, Meyer R, Philippy R, Samama JC (1990) Role of aluminium in the structure of Brazilian opals. Eur J Mineral 2:611–619

Beccaluva L, Bianchini G, Natali C, Siena F (2009) Continental flood basalts and mantle plumes: a case study of the Northern Ethiopian plateau. J Petrol 50(7):1377–1403

Berhe SM, Desta B, Nicoletti M, Tefera M (1987) Geology, geochronology and geodynamic implications of the Cenozoic magmatic province in W and SE Ethiopia. J Geol Soc Lond 144:213–226

Campbell KA, Guido DM, Gautret P, Foucher F, Ramboz C, Westall F (2015) Geyserite in hot-spring siliceous sinter: window on Earth’s hottest terrestrial (paleo) environment and its extreme life. Earth Sci Rev 148:44–64. https://doi.org/10.1016/j.earscirev.2015.05.009

Caucia F, Marinoni L, Leone A, Adamo I (2013) Investigation on the gemmological, physical and compositional properties of some opals from Slovakia (“Hungarian” opals). Period Di Mineral 82(2):251–261

Chauviré B, Rondeau B, Mazzero F, Ayalew D (2017) The precious opal deposit at Wegel Tena, Ethiopia: formation via successive pedogenesis events. Can Mineral 55(4):701–723

Chauviré B, Rondeau B, Alexandre A, Chamard-Bois S, La Carole C, Mazzero F (2019) Pedogenic origin of precious opals from Wegel Tena (Ethiopia): evidence from trace elements and oxygen isotopes. Appl Geochem 101:127–139

Clarke JDA (2003) The occurrence and significance of biogenic opal in the regolith. Earth Sci Rev 60(3–4):175–194

Coulie E, Quideleur X, Gillot PY, Courtillot V, Lefèvre JC, Chiesa S (2003) Comparative K-Ar and Ar/Ar dating of Ethiopian and Yemenite Oligocene volcanism: implications for timing and duration of the Ethiopian traps. Earth Planet Sci Lett 206:477–492

Curtis NJ, Gascook JR, Johnson MR, Pring A (2019) A review of the classification of opal with reference to recent new localities. Minerals 9(5):299. https://doi.org/10.3390/min9050299

Day R, Jones B (2008) Variations in water content in opal-A and opal-CT from geyser discharge aprons. J Sediment Res 78(4):301–315. https://doi.org/10.2110/jsr.2008.030

Dowell K, Mavrogenes J, McPhail DC, Watkins JJ (2002) Origin and timing of formation of precious black opal nobbies at Lightning Ridge. In: Roach IC (ed) Regolith and Landscapes in Eastern Australia. CRC LEME, Perth, pp 18–20

Dutkiewicz A, Landgrebe TCW, Rey PF (2015) Origin of silica and fingerprinting of Australian sedimentary opals. Gondwana Res 27:786–795

Ebinger CJ, Sleep NH (1998) Cenozoic magmatism throughout East Africa resulting from impact of a single plume. Nature 395:788–791. https://doi.org/10.1038/27417

Ebinger CJ, Yemane T, WoldeGebriel G, Aronson JL, Walter RC (1993) Late Eocene-recent volcanism and faulting in the southern main Ethiopian rift. J Geol Soc London 150:99–108

Eckert AW (1997) The world of opals. Jone and Wiley & Son, INC, New York and Chichester, pp 448

Elzea JM, Rice SB (1996) TEM and X-ray diffraction evidence for cristobalite and tridymite stacking sequences in opal. Clays Clay Miner 44:492–500

Fritsch E, Rondeau B (2009) Gemology: the developing science of gems. Elements 5:147–152

Fröhlich, (2020) The opal-CT nanostructure. J Non Cryst Solids 533(2):1–8. https://doi.org/10.1016/j.jnoncrysol.2020.119938

Gaillou E, Delaunay A, Rondeau B, Bouhnik-le-Coz M, Fritsch E, Cornen G, Monnier C (2008) The geochemistry of gem opals as evidence of their origin. Ore Geol Rev 34(1–2):113–126

Gallacher AD (2001) Geochemistry of sedimentary opal, Hebel, Southern Queensland (unpublished Doctoral thesis). School of Earth Sciences, Melbourne Vic: The University of Melbourne

Gauthier JP, Mazzero F, Mandaba Y, Fritsch E (2004) Opal from Ethiopia: usual gemology and unusual characteristics. Rev Gemmol AFG 149:15–23

George R, Rogers N, Kelley S (1998) Earliest magmatism in Ethiopia: evidence for two mantle plumes in one flood basalt province. Geology 26:923–926

Goryniuk MC, Rivard BA, Jones B (2004) The reflectance spectra of opal-A (0.5–25μm) from the Taupo Volcanic Zone: spectra that may identify hydrothermal system on planetary surfaces. Geophys Res Lett 31:L24701. https://doi.org/10.1029/2004GL021481

Gübelin E (1986) Les opales mexicaines. Revue de Gemmologie (a.f.g.) 88:3–8

Guthrie GD, Bish DL, Reynolds RC (1995) Modelling the X-ray diffraction pattern of opal-CT. Am Mineral 80:869–872

Harnois L (1988) The CIW index: a new Chemical Index of Weathering. Sediment Geol 55:319–322

Hofmann C, Courtillot V, Feraud G, Rochette P, Yirgu G, Ketefo E, Pik R (1997) Timing of the Ethiopian flood basalt event and implications for plume birth and global change. Nature 389:838–841

Iler RK (1979) The chemistry of silica: solubility, polymerization, colloid and surface properties and biochemistry of silica. John Wiley and Sons, New York, NY

Johnson ML, Kammerling RC, DeGhionno DG, Koivula JI (1996) Opal from Shewa Province. Ethiopia Gems Gemol 32(2):112–120

Jones B, Renaut RW (2004) Water content of opal-A: implications for the origin of laminae in geyserite and sinter. J Sediment Res 74(1):117–128

Jones JB, Segnit ER (1971) Nature of opal part I: nomenclature and constituent phases. J Geol Soc Aust 18:57–68

Kiefert L, Hardy P, Sintayehu T, Abate B, Woldetinsae G (2014) A new deposit of black opal from Ethiopia. Gems Gemol 50(4):302–315

Kieffer B, Arndt N, Lapierre H, Bastien F, Bosch B, Pecher A, Yirgu G, Ayalew D, Weis D, Jerram DA, Keller F, Meugniot C (2004) Flood and shield basalts from Ethiopia: magmas from the African superswell. J Petrol 45:793–834

Koivula JI, Fryer CW, Keller CP (1983) Opal from Queretaro, occurrence and inclusions. Gems Gemol 19(2):87–98

Langer K, Flörke OW (1974) Near infrared absorption spectra (4000–9000 cm-1) of opals and the role of “water” in these SiO2-nH2O minerals. Fortschr Mineral 52:17–51

Le Bas MJ, LeMaitre RW, Streckeisen A, Zanettin B (1986) A chemical classification of volcanic rocks based on the total alkali-silica diagram. J Petrol 27(3):745–750

Liang Y, Zhang J, Liu Y, Tang X, Li Z, Ding J, Wang Y, Yang S (2020) Evidence for biogenic silica occurrence in the lower Silurian Longmaxi Shale in Southeastern Chongqing. China Minerals 10(11):945. https://doi.org/10.3390/min10110945

Liesegang M, Milke R (2014) Australian sedimentary opal-A and its associated minerals: implications for natural silica sphere formation. Am Mineral 99:1488–1499

Lynne BY, Campbell KA, Moore JN, Browne PRL (2005) Diagenesis of 1900-year old siliceous sinter (opal-A to quartz) at Opal Mound, Roosevelt Hot Springs, Utah. U.S.A. Sediment Geol 179:249–278. https://doi.org/10.1016/j.sedgeo.2005.05.012

Martin E, Gaillou E (2018) Insight on gem opal formation in volcanic ash deposits from a supereruption: a case study through oxygen and hydrogen isotopic composition of opals from Lake Tecopa, California, U.S.A. Am Min 103:803–811. https://doi.org/10.2138/am-2018-6131

Mazzero F, Gauthier JP, Rondeau B, Fritsch E, Bekele E (2009) Nouveau gisement d’opales d’Ethiopie dans la Province du Welo: Premières informations. [New deposit of Ethiopian opals in the Wollo Province: Early information]. Revue de Gemmologie a.f.g. 167:4–5 [in French]

McOrist GD, Smallwood AG, Fardy JJ (1994) Trace elements in Australian opals using neutron activation analysis. J Radioanal Nucl Chem 185:293–303

Merla G, Abbate E, Azzaroli A, Bruni P, Canuti P, Fazzuoli M, Sagr M, Tacconi P (1979) A geological map of the Ethiopia and Somalia and comment with a map of major landforms (scale 1:2,000,000). Consiglio Nazionale delle Ricerche, Frienze Italy, pp 95

Meshesha D, Shinjo R (2007) Crustal contamination and diversity of magma sources in the northwestern Ethiopia volcanic province. J Mineral Petrol Sci 102:272–290

Natali C, Beccaluva L, Bianchini G, Siena F (2016) Comparison among Ethiopia- Yemen, Deccan, and Karoo continental flood basalts of central Gondwana: insights on lithosphere versus asthenosphere contributions in compositionally zoned magmatic provinces. Spec Pap Geol Soc Am 526:191–215

Nesbitt HW, Young GM (1982) Early Proterozoic climates and plate motions inferred from major element chemistry of lutites. Nature 299:715–717

Peucat JJ, Ruffault P, Fritsch E, Bouhnik-le coz M, Simonet C, Lasnier B (2007) Ga/Mg ratio as a new geochemical tool to differentiate magmatic from metamorphic blue sapphires. Lithos 98:261–274

Pik R, Deniel C, Coulon C, Yirgu G, Hofmann C, Ayalew D (1998) The northwestern Ethiopian plateau flood basalts: classification and spatial distribution of magma types. J Volcanol Geotherm Res 81(1–2):91–111

Pik R, Daniel C, Coulon C, Yirgu G, Marty B (1999) Isotopic and trace element signatures of Ethiopian flood basalts: evidence for plume lithosphere interactions. Geochim Cosmochim Acta 63(15):2263–2279

Pirajno F (2009) Hydrothermal processes and mineral system. Springer Berlin Germany, pp 1250. https://doi.org/10.1007/978-1-4020-8613-7

Rey PF (2013) Opalisation of the Great Artesian Basin (central Australia): an Australian story with a Martian twist. Aust J Earth Sci 60:291–314

Rodgers KA, Browne PRL, Buddle TF, Cook KL, Greatrex RA, Hampton WA, Herdianita NR, Holland GR, Lynne BY, Martin R, Newton Z, Pastars D, Sannazarro KL, Teece CIA (2004) Silica phases in sinters and residues from geothermal fields of New Zealand. Earth Sci Rev 66(1–2):1–61. https://doi.org/10.1016/j.earscirev.2003.10.001

Rondeau B, Fritsch E, Fritsch M, Renac C (2004) Opals from Slovakia (“Hungarian” opals): a re-assessment of the conditions of formation. Eur J Mineral 16:789–799

Rondeau B, Fritsch E, Mazzero F, Gauthier JP, Cenki-Tok B, Bekele E, Gaillou E (2010) Play-of-color Opal from Wegel Tena, Wollo Province. Ethiopia Gems Gemol 46(2):90–105
Rondeau B, Cenki-Tok B, Fritsch E, Mazzero F, Gauthier JP, Bodeur Y, Bekele E, Gaillou E, Ayalew D (2012) Geochemical and petrological characterization of gem opals from Wegel Tena, Wollo, Ethiopia: opal formation in an Oligocene soil. Geochem Explor Environ 12(2):93–104
Rossman GR (2009) The geochemistry of gems and its relevance to gemology: different traces, different prices. Elements 5:159–162
Shigley JE, Laurs BM, Renfro ND (2009) Chrysoprase and prase opal from Haneti, Central Tanzania. Gems Gemol 45:271–279
Simoni M, Caucia F, Adamo I, Galinetto P (2010) New occurrence of fire opal from Bemia, Madagascar. Gems Gemol 46:114–121
Smallwood A, Thomas PS, Ray AS (1997) Characterisation of sedimentary opals by Fourier transform Raman spectroscopy. Spectrochim 53:2341–2345
Smallwood A, Thomas PS, Ray A (2008) Comparative Analysis of Sedimentary and Volcanic Precious Opals from Australia. J Aust Ceram 44(2):17–22
Sun SS, McDonough WF (1989) Chemical and isotopic systematics of oceanic basalts: implications of mantle composition and processes. Geol Soc Spec Publ 42(1):313–345
Thiry M, Simon-Coinçon R (1996) Tertiary paleoweatherings and silcretes in the southern Paris Basin. CATENA 26:1–26
Thiry M, Milnes AR, Rayot V, Simon-Coinçon R (2006) Interpretation of palaeoweathering features and successive silicifications in the tertiary regolith of inland Australia. J Geol Soc London 163:723–736
Ukstins IA, Renne PR, Wolfenden E, Baker J, Ayalew D, Menzies M (2002) Matching conjugate volcanic rifted margins: 86 40Ar/39Ar chrono-stratigraphy of pre and syn-rift bimodal flood volcanism in Ethiopia and Yemen. Earth Planet Sci Lett 198(3–4):289–306
Ullyott JS, Nash DJ, Whiteman CA, Mortimore RN (2004) Distribution, petrology and mode of development of silcretes (sarsens and puddingstones) on the eastern South Downs, UK. Earth Surf Process Landf 29:1509–1539
Wilson J (2014) The structure of opal-CT revisited. J Non Cryst Solids 405(1):68–75. https://doi.org/10.1016/j.jnoncrysol.2014.08.052
Winchester JA, Floyd PA (1997) Geochemical discrimination of different magma series and their differentiation products using immobile elements. Chem Geol 20:245–252
Wolfenden E, Ebinger C, Yirgu G, Deino A, Ayalew D (2004) Evolution of the northern Main Ethiopian rift: birth of a triple junction. Earth Planet Sci Lett 224:213–228
Yu XY (2009) Colored gemmology, 2nd edn. Geological Publishing House, Beijing, China, p 10
Zewdie S, Mammo W, Negassa G (2009) Opportunities for gem resource development in Ethiopia. EIGS, unpublished promotion report, Addis Ababa, Ethiopia, pp 31